Fusion Engineering and Design 193 (2023) 113661

Contents lists available at ScienceDirect

Fusion Engineering and Design

journal homepage: www.elsevier.com/locate/fusengdes

First measurements of a scintillator-based fast-ion loss detector in reversed I_p/B_t at the ASDEX Upgrade tokamak

J. Hidalgo-Salaverri [a,*], J. Rueda-Rueda [b], J. Galdon-Quiroga [b], P. Cano-Megias [c], E. Viezzer [b], J. Garcia-Dominguez [b], D. Silvagni [d], M. Videla-Trevin [e], P. Oyola [b], J. Ayllon-Guerola [a], M. Garcia-Munoz [b], T. Happel [d], the ASDEX Upgrade Team

[a] Department of Mechanical Engineering and Manufacturing, University of Seville, Seville, Spain
[b] Department of Atomic, Molecular and Nuclear Physics, University of Seville, Seville, Spain
[c] Department of Energy Engineering, University of Seville, Seville, Spain
[d] Max-Planck-Institut für Plasmaphysik, Garching, Germany
[e] Department of Materials and Transport Science and Engineering, University of Seville, Spain

A B S T R A C T

Fast-α losses in future fusion power plants are expected to follow the co- and counter-current directions due to the isotropy of the fusion reaction. At the ASDEX Upgrade tokamak, the co-current direction (achieved with positive plasma current and negative toroidal magnetic field) has been extensively studied thanks to an array of five fast-ion loss detectors (FILD). A new fast-ion loss detector compatible with reversed I_p/B_t (negative plasma current and positive magnetic toroidal field, defining positive as counter-clockwise when the machine is viewed from the top), namely RFILD, has been designed and commissioned to study the behaviour of counter-current fast-ion losses and to expand our knowledge on QH-mode, I-mode, and the L-H transition. The detector is a modified version of the midplane manipulator fast-ion loss detector that features a new probe head orientation and collimator geometry, optimised using the FILDSIM code. A fast CMOS camera is used as a high spatial resolution acquisition system, while an array of photomultipliers (up to 1 MHz) serves as a fast channel.

First measurements have been taken in I-mode, QH-mode, L-mode and H-mode with core densities ranging between $4{\cdot}10^{19}$ and $9{\cdot}10^{19}$ m^{-3}, I_p between -0.8 and -0.6 MA and B_t of 2.5 T approximately. NBI fast-ion losses were observed for the first time in reversed I_p/B_t, producing high pitch (60 – 80°) losses. ICRH losses in H-minority heating configuration have also been observed in I-mode experiments. These losses correspond to the outer leg of banana particle trajectories. An upgraded double collimator detector design is also presented, that will increase the measurable particle range in future experimental campaigns (co- and counter-current particles simultaneously). Thus, we expand our understanding on the mechanisms behind fast-ion losses at the ASDEX Upgrade tokamak in the reversed I_p/B_t configuration.

1. Introduction

Fast-ion confinement is essential to maintain burning plasmas and to avoid damaging plasma facing components in future fusion reactors. The scintillator-based fast-ion loss detector (FILD) is used in several fusion experiments [1–3] to diagnose the mechanisms behind the loss of these energetic particles. In the ASDEX Upgrade tokamak (AUG), a total of five FILDs are installed in different poloidal positions providing a good space coverage in forward I_p/B_t [1,4,5]. Due to the detector geometry, these detectors can only provide measurements in forward I_p/B_t configuration. In this work, a reversed I_p/B_t-compatible FILD, named RFILD (Reversed I_p/B_t Fast-Ion Loss Detector) is presented.

In future fusion power plants, fast ions can be expected in co- and counter- current trajectories due to the isotropy of the alpha particles from the fusion reaction. At ASDEX Upgrade, FILD systems present a single collimator that is orientated to measure co-current fast-ion losses (FIL) to maximise the signal as NBI sources are built to produce co-current fast ions. As the NBI injection is counter-current in reversed I_p/B_t, this opens the possibility of studying the behaviour of counter-current fast ions that make half of the α population at birth in ITER and DEMO.

In the ASDEX Upgrade tokamak, the forward/reversed I_p/B_t configuration is characterised for featuring a positive/negative plasma current and a negative/positive toroidal magnetic field (positive direction is defined as shown in Fig. 1(a)). NBI injection is counter-current in reversed I_p/B_t as the NBI geometry is designed to be co-current in forward I_p/B_t and it cannot be changed. This enables the study of different confinement regimes that present interesting properties in this configuration like the I-mode (reversed I_p/B_t allows for lower single null plasmas, while in forward I_p/B_t can only be reached in upper single null

* Corresponding author.
E-mail address: jhsalaverri@us.es (J. Hidalgo-Salaverri).

https://doi.org/10.1016/j.fusengdes.2023.113661
Received 31 October 2022; Received in revised form 9 February 2023; Accepted 15 March 2023
Available online 20 March 2023

due to the ∇B drift direction) [6], QH-mode [7,8] and L-H transition studies.

The resulting NBI population features a worse confinement than their forward I_p/B_t counterpart. The extra losses in reversed I_p/B_t might be explained by the resulting trajectories in this counter current scenario where the trapped particles are injected in the inner leg of banana orbits, thus, closing outwards. An example of a trapped and a passing orbit in forward and reversed I_p/B_t is shown in Fig. 1(a). Here, it can be seen how the ∇B drift direction varies between the forward (downwards for ions) and reversed I_p/B_t configuration (upwards for ions). This motivates that the banana orbits close outwards in reversed I_p/B_t and inwards in forward I_p/B_t. Therefore, the banana orbits in reversed I_p/B_t can easily collide with the plasma facing components as shown in Fig. 1(a), increasing the NBI losses in this configuration. ASCOT [9] simulations in Fig. 1(b) confirm how the NBI losses are larger in reversed I_p/B_t for all 8 NBIs available in AUG. The simulated scenarios correspond to a pair of shots with the same absolute toroidal magnetic field of 2.5 T and plasma current of 1.0 MA and a similar plasma shape; at the simulated time-point, both shots feature 5 MW of external heating.

This paper is structured as follows. In Section 2, the diagnostic motion and acquisition system together with the collimator optimisation are introduced. Section 3 presents the commissioning strategy and the first measurements. Section 4 describes a future double collimator RFILD, followed by the conclusions in Section 5.

2. Diagnostic setup

The scintillator-based fast-ion loss detectors can be thought of as magnetic spectrometers that use the local magnetic field to disperse ions onto a scintillator plate. In ASDEX Upgrade, the detector is composed by a probe head, a collimator, and a scintillator as in-vessel components. The probe head serves as a heat shield and blocks the entrance of undesired particles and light into the system. The collimator determines the combinations of gyroradius (ρ_L) and pitch angle (defined as $\Lambda = \arccos\left(\frac{v_{||}}{v}\right)$, being $v_{||}$ parallel to the plasma current) that are accepted into the scintillator. The strike point of the incoming particle reveals its energy and Λ. The light emitted is captured by a train of lenses that carry the signal to two acquisition systems thanks to a beam splitter. A fast CMOS camera is used as the high-resolution system (800 × 600 pixels at ~1 kHz with a resolution in gyroradius of 0.05–0.1 cm/pixel and of 0.4–0.8°/pixel in pitch. Resolution decays with gyroradius), while an array of photomultipliers acts as the high-speed system (up to 1 MHz). The high-speed acquisition system allows for the study of the interaction between fast-ion losses and MHD events [1].

RFILD has been mounted on the midplane manipulator of the ASDEX Upgrade tokamak, located approximately 30 cm above the midplane. Mechanically, RFILD is a modified version of FILD1 [1], a forward configuration fast-ion loss detector. This is, a new collimator was added and the in-vessel components (probe head, collimator, scintillator, and their support structures) were rotated until the collimator was aligned with the local magnetic field in reversed I_p/B_t configuration to maximise the incoming flux of fast ions and the resolution. As shown in Fig. 2(a) and (b), reversed I_p/B_t orbits reach the probe head from below, thus motivating said probe head rotation. The motion system, probe head and acquisition systems of FILD1 and RFILD are shared.

The midplane manipulator can be adjusted radially in between shots. RFILD is toroidally located behind a limiter that protects the detector, but, at the same time, blocks the incoming fast-ion losses. Therefore, a good positioning of the probe head is essential in a FILD detector, to ensure a compromise position between the measurements and the received heat loads. A lead screw is used for the radial movement, with a precision of 0.01 m.

The FILDSIM [10,11] code has been used to optimise the collimator geometry. The collimator geometry defines the accepted particle population as well as the resolution for each energy-pitch combination. This code starts Monte Carlo markers on the pinhole with different pitch- ρ_L combinations, each marker corresponds to a particle with these characteristics that is assumed to follow a helix. This assumption has been checked to be close enough to a full orbit simulation as the simulated particle only travels for a few periods. The forward tracing of the particles provides the strikemap of the incoming fast ions, while the backward tracing considers the effect of the probe head geometry (particles blocked by the probe head itself, this phenomenon is known as self-shadowing) over the strikemap.

In reversed I_p/B_t configuration, the bulk of the expected fast-ion losses belong to the outer leg of the banana trajectories. Therefore, trapped particles with a 45 – 90° Λ range could reach the detector. In terms of ρ_L, the ASDEX Upgrade tokamak has 4 NBIs with an injection energy of 60 keV (sources 1 to 4) and another 4 of 93 keV (sources 5 to 8) for deuterium. Higher energies in the MeV range can be expected from ICRH-induced losses. The resolution of the main energy injection of the high energy beams (93 keV) has been optimised, as the ρ_L resolution gets coarser for larger gyroradii and significant prompt losses have been measured in other FILD detectors in AUG [1]. This translates to ~33 mm in ρ_L when considering a magnetic field on axis of 2.5 T (1.88 T on the probe head), the standard field on AUG.

Fig. 2(c) shows the main in-vessel components of the detector. The working mechanism of the collimator is presented here. The collimator

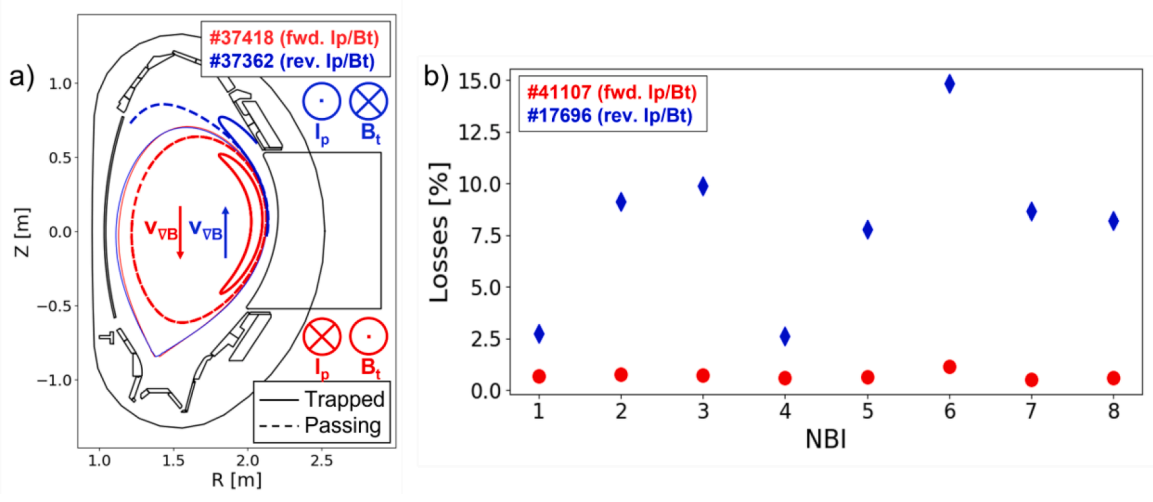

Fig. 1. (a) Poloidal cross-section of AUG with trapped and passing trajectories for a forward (#37418 in red) and reversed (#37362 in blue) scenario. (b) NBI losses estimated by ASCOT in forward I_p/B_t (#17696 in blue) and in reversed I_p/B_t (#41107 in red). b.

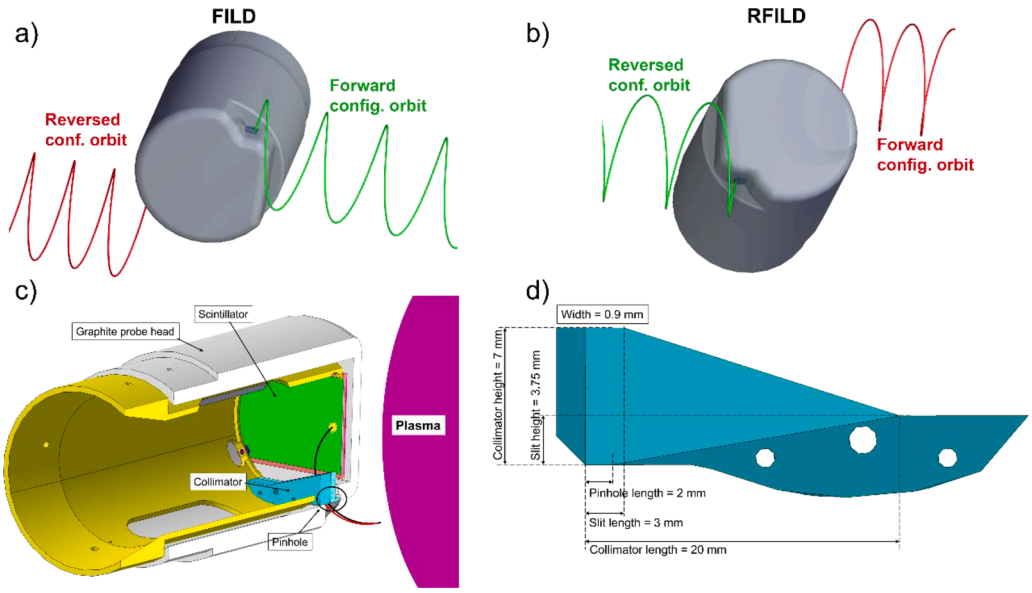

Fig. 2. (a) FILD and (b) RFILD probe head orientation. Orbits in reversed and forward I_p/B_t are added. Accepted orbits in green, rejected in red. (c) RFILD main in-vessel components. (d) Collimator geometry.

geometry allows the entrance of a certain population of fast ions (in black) while blocking other particles (in red) and light coming from the plasma. The geometry parameters studied with the FILDSIM code are shown in Fig. 2(d). The collimator height affects the ρ_L resolution by narrowing/broadening the gyrophase cone accepted by the collimator when this length is increased/decreased. A wider gyrophase cone means a larger spread in the resulting spot which penalises the resolution but improves the intensity of the signal. The slit height, length and the collimator length mainly affect the accepted Λ. The pinhole length and the collimator width influence both on the ρ_L and Λ. It is important to note that all these parameters are strongly related, therefore, varying one modifies how the others affect the end resolution. Thus, a scan in all variables was done with the resolution at 33 mm as the objective function. The resulting geometry values are shown in Fig. 2(d).

Fig. 3 shows the ρ_L and Λ resolution of the optimised RFILD collimator. The detector resolutions are assumed to follow a Gaussian (for the pitch resolution) or a skewed Gaussian (for the ρ_L resolution) fitted to the modelled markers. The ρ_L at a pitch of 80° has been shown as the expected population of fast-ion losses are mostly trapped particles. In the Λ resolution case, the case at 3.0 cm has been selected as it approximately corresponds to the NBI main injection energy. The Λ resolution is fairly constant for every ρ_L, while the Gaussian width of the ρ_L resolution increases for large ρ_L orbits.

3. First measurements

The commissioning and first measurements of the RFILD diagnostic were carried out during the 2021 reversed I_p/B_t configuration campaign at the ASDEX Upgrade tokamak in a series of shots with core densities ranging between $4{\cdot}10^{19}$ and $9{\cdot}10^{19}$ m^{-3}, I_p between -0.8 and -0.6 MA and B_t of 2.5 T. During this campaign, RFILD measured under different regimes, namely, QH-mode, I-mode, and L-H transition studies. The commissioning and first measurements in reversed I_p/B_t configuration of NBI and ICRH fast-ion losses, and NTM (a neoclassical tearing mode) induced fast-ion losses are presented below. A more in depth analysis of the I-mode shots, together with the QH-mode and L-H transition experiments will be discussed in a future publication.

3.1. Commissioning

The scintillating material used, TG-green, has to be maintained below ~200 °C for a good operation, as its efficiency decreases at greater temperatures [12]. Therefore, a low scintillator temperature is essential for an optimal operation. At the same time, the probe head, as a plasma facing component, can receive significant heat loads [13]. To keep the scintillator cool under these conditions, the scintillator is not in contact with the graphite probe head and is kept in place by the head support structure. The ASDEX Upgrade tokamak features a series of infrared cameras that monitors the first wall and the divertor [14]. During the RFILD commissioning, one of these cameras was focused on

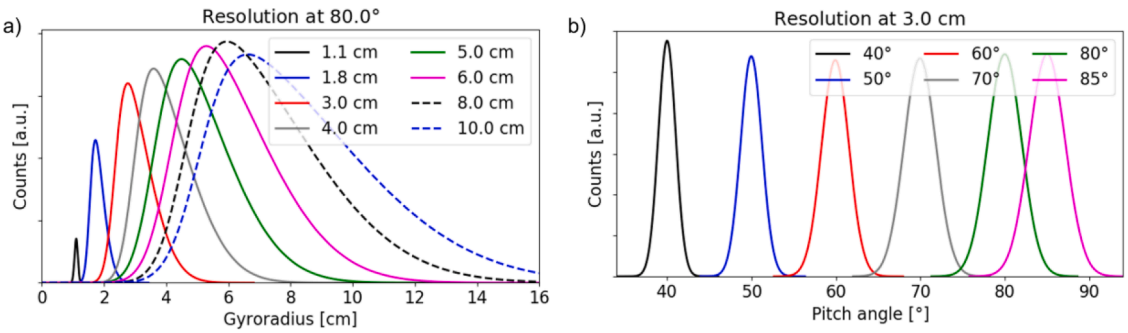

Fig. 3. (a) ρ_L resolution fit at $\Lambda = 80°$. (b) Λ resolution fit at $\rho_L = 3.0$ cm.

RFILD to control the probe head temperature as it was further inserted in each new shot. The commissioning was accomplished in a series of NBI scan shots (#38669 – #38673) with a toroidal field of 2.5 T and a plasma current of −0.6 MA. Fig. 4 shows the (a) time trace of the probe head maximum temperature and (b) the infrared camera view of the detector head. Fig. 4 corresponds to shot #38673, where RFILD was at the maximum insertion reached during the commissioning and the distance to the plasma was at its minimum (~8 cm). The probe head temperature rises in each NBI phase probably due to the energy deposited by the FIL that reach the graphite probe head. When the NBI turns off, the temperature rapidly decreases as the energy is diffused over the rest of the probe head material. The temperature peak at around 5.9 s corresponds to the end of the shot. This peak may be an artefact caused by some sudden reflection of the disrupting plasma or the surrounding structures on the tungsten covered graphite probe head. The integrity of the probe head is governed by the graphite sublimation temperature [15], this is 2000°C for the used graphite (isostatically pressed R6710 graphite) [16]. The maximum temperature reached on the probe head surface was ~150°C, therefore, the temperature at the scintillator was much lower and the emission efficiency was not jeopardized. Fig. 4(b) shows the RFILD probe head (with the overlayed CAD) in a time point when NBI #7 was on; it can be observed that the lower region is the hottest part of the system. This is to be expected, as it is the closest point to the plasma and, as previously stated, most FIL will reach the probe head from below.

3.2. NBI losses

An NBI scan was performed in shot #38673. During this shot, sources 2 to 7 were used. Fig. 5 presents a series of time traces corresponding to this shot. Fig. 5(a) shows the RFILD signal time trace, (b) and (c) the heating scheme together with the radiated plasma power and (d) the evolution of the edge and core electron temperature and density. The NBI scan starts at 2.0 s, the ECRH is kept constant during the whole scan and the electron temperature and density are fairly constant except for a spike at the beginning due to the sudden increase in the input power motivated by the onset of NBI #6 and a step in ECRH power. Each NBI was turned on for 200 ms with a no-NBI period between them of 150 ms. At the end of this scan, NBI#7 was pulsed (8 ms on/15 ms off) for half a second, followed by another half a second of constant NBI injection. There is a clear correlation between the usage of NBIs and the appearance of fast-ion losses. NBI#8 deposits the largest number of losses in RFILD, followed by NBI#5 and NBI#2. The rest of sources produce a similar level of signal, except for NBI#6 which was switched on during a time period where the electron temperature and density was still evolving. It is interesting to note the qualitative difference between these results and ASCOT simulations shown in Fig. 1; RFILD obtains local measurements of the FIL population while the ASCOT simulations consider the whole lost population.

The different NBIs leave a different footprint on the scintillator. NBIs #6 and #7 produced a single spot, while the rest of sources (#2, #3, #4, #5 and #8), two. This is pictured in Fig. 6, where the time averaged signal of two time periods with NBI#7 (Fig. 6(a)) and NBI#5 (Fig. 6(b)) are shown. Both frames show a common high pitch spot (~85°, trapped particles) with a ρ_L ~2.1 cm. The NBI#5 case also features a second spot centred around 60° (passing particles) and ~1.6 cm. This spot has been identified as prompt-losses from NBI#5 as the Λ is compatible with the injected ions from this source and the onset/offset of the RFILD signal occurs on the μs scale after the beam is turned on/off. Sources #2, #3, #4 and #8 follow the same behaviour as NBI#5 with small variations in pitch.

3.3. ICRH losses

ICRH fast-ion losses were consistently measured in a series of shots with 2.5 T and a plasma current of −0.8 MA. Here, shot #38686 is presented as an example as it shows the clearest signal and dynamics in the RFILD detector. Other shots in these studies (i.e., #38684) behave similarly.

Fig. 7 shows a series of time traces corresponding to #38686. The RFILD signal time trace (Fig. 7(a)) has been obtained by integrating two different regions of interest. The low- ρ_L losses (in black) correspond to the area below 4.5 cm, while the high-ρ_L losses (in blue) encompass the signal from more than 4.5 cm for the whole Λ range. These regions can be seen in Fig. 8(a) where a CMOS camera frame with an overlayed strikemap is shown. Fig. 7(b) and (c) show the heating scheme. In this shot, the ICRH was working in the minority H-heating scheme. This means that the ICRH frequency was set at the main ion cyclotron frequency of hydrogen, the minority species in a deuterium plasma. NBI deuterium ions will also be heated as the main harmonic of hydrogen coincides with the second harmonic of deuterium [17]. Fig. 7(d) shows the time evolution of the electron temperature and density at the edge and the core.

The start of the ICRH ($t = 1.0$ s) triggers low-energy losses followed by high-energy ones. These are losses of hydrogen fast ions at energies of 107 keV and 1203 keV respectively, as no NBI was active during this time period. The losses get significantly mitigated as the electron temperature and density stabilise, until the ICRH power is increased at t ~ 1.9 s which produces more low-energy hydrogen losses. From ~4.5 s onwards, some cyclic high-ρ_L losses can be observed that are correlated with NBI#2 (60 keV of main injection energy) and with changes in the electron temperature and density. Fig. 8(a) shows a frame corresponding

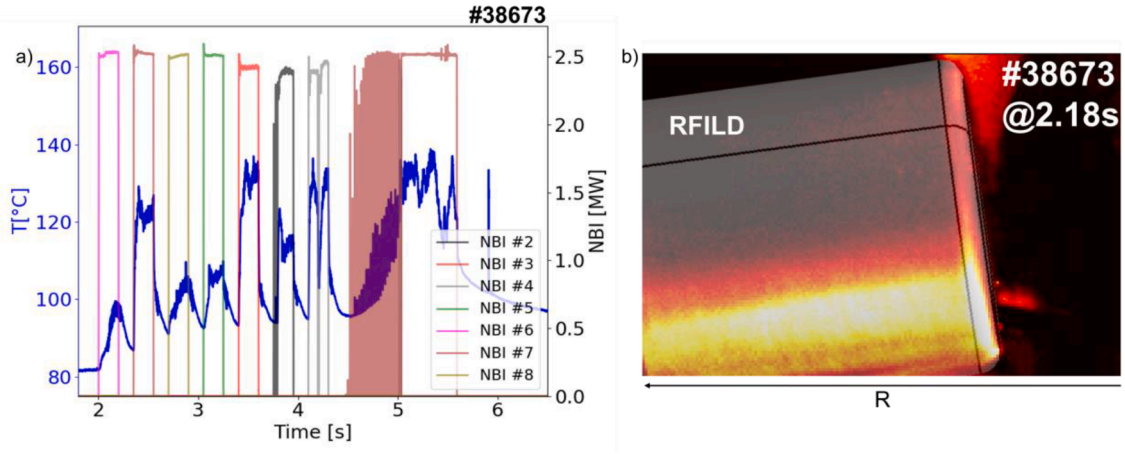

Fig. 4. a) Probe head temperature evolution with NBI time traces for #38,673. b) View of the RFILD probe head by the IR camera. The probe head CAD model has been overlayed.

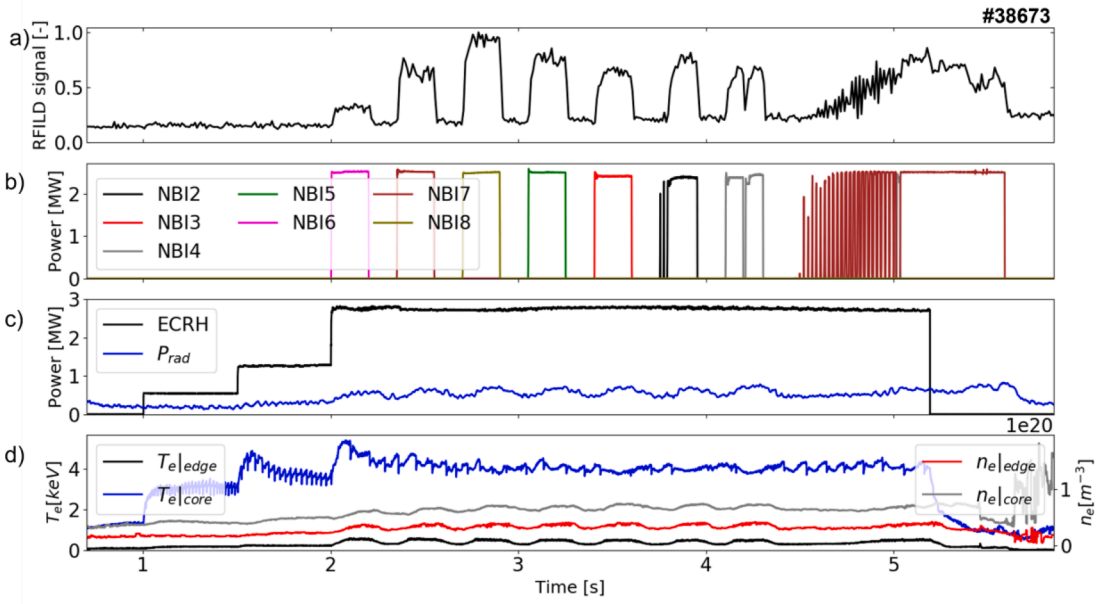

Fig. 5. Time traces corresponding to #38673: (a) RFILD signal, (b) NBI heating, (c) ECRH and radiated plasma power, (d) electron temperature and density at the edge and the core.

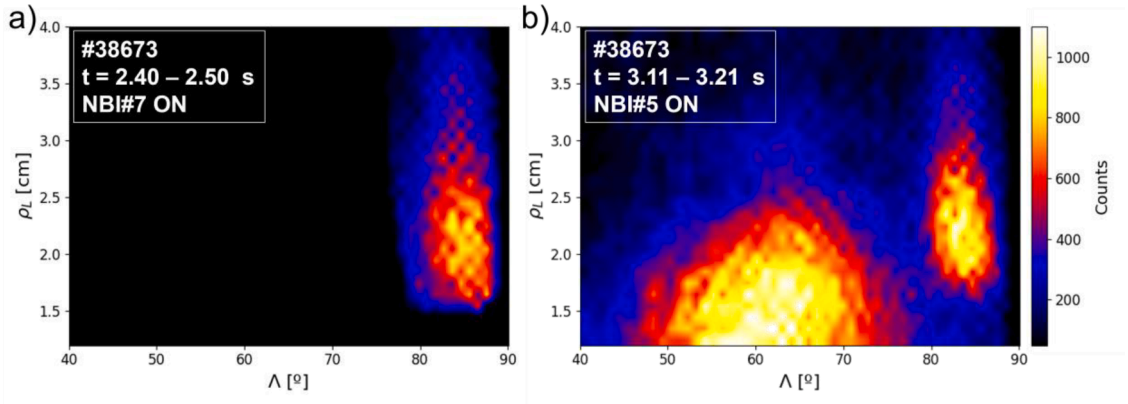

Fig. 6. Remapped RFILD signal. (a) Averaged signal between 2.40 and 2.50 s, when NBI#7 was on. (b) Averaged signal between 3.11 and 3.21 s, when NBI#5 was on.

to $t = 4.72$ s, where the ICRH and NBI#2 were on. Two spots can be easily distinguished in this figure. The low-ρ_L spot, ranging from 1.4 to 4.2 cm, could have originated from main injection energy deuterons or from ICRH hydrogen as it shares the same position as the hydrogen spot found in the absence of NBI. Modelling is required to disentangle the contributions from each source, and it is left for a follow-up publication. The high-ρ_L spot (located between 4.8 and 10.8 cm) arises due to ICRH ions. Fig. 9(b) shows an orbit traced back from the diagnostic pinhole with the spot pitch and ρ_L. It can be seen that the tips of the resulting banana are located at the ICRH resonant layer. This confirms that these are indeed ICRH induced fast-ion losses but does not provide information about the species. Therefore, this could be hydrogen losses of 860 keV or deuterium ions of 420 keV.

3.4. NTM induced losses

In #38686, a neoclassical tearing mode (NTM) was measured by RFILD as it can be observed in Fig. 7(g). In this figure, the magnetics signal is compared against the RFILD spectrogram showing how the NTM visible in the magnetics also appears in the 5.90 – 6.10 s time window in the RFILD spectrogram. The analysis of the electron cyclotron emission diagnostic shows that the mode is located in the region ρ_{pol} ~0.3 – 0.5 during its appearance in the RFILD spectrogram. The analysis of pick-up coils suggest that it is a $m = 2$, $n = 1$ NTM sitting at $q = 2$. The NTM-modulated losses appeared in the scintillator as a spot at $\Lambda \sim 85°$ and $\rho_L \sim 2.5$ cm. The temporal correlation with the NBI7 suggest that these are prompt losses that interact with the NTM before getting to RFILD.

4. Double collimator configuration

As presented in Section 2, the current single collimator configuration allows for the measurement of trapped particles originating the outer leg of banana orbits. A double collimator, similar to the TCV design [18], is proposed to further expand the detector measuring capabilities. This second collimator faces the counter-current direction, where it is expected to intersect with the inner leg of banana trajectories and passing particles. This allows for the simultaneous measurement of FIL coming from the co- and counter-current direction. This capability is essential for future tokamaks like ITER where the α particles may come from both directions. Both collimators in this configuration follow the design shown in Section 2, therefore, the expected resolution can be observed

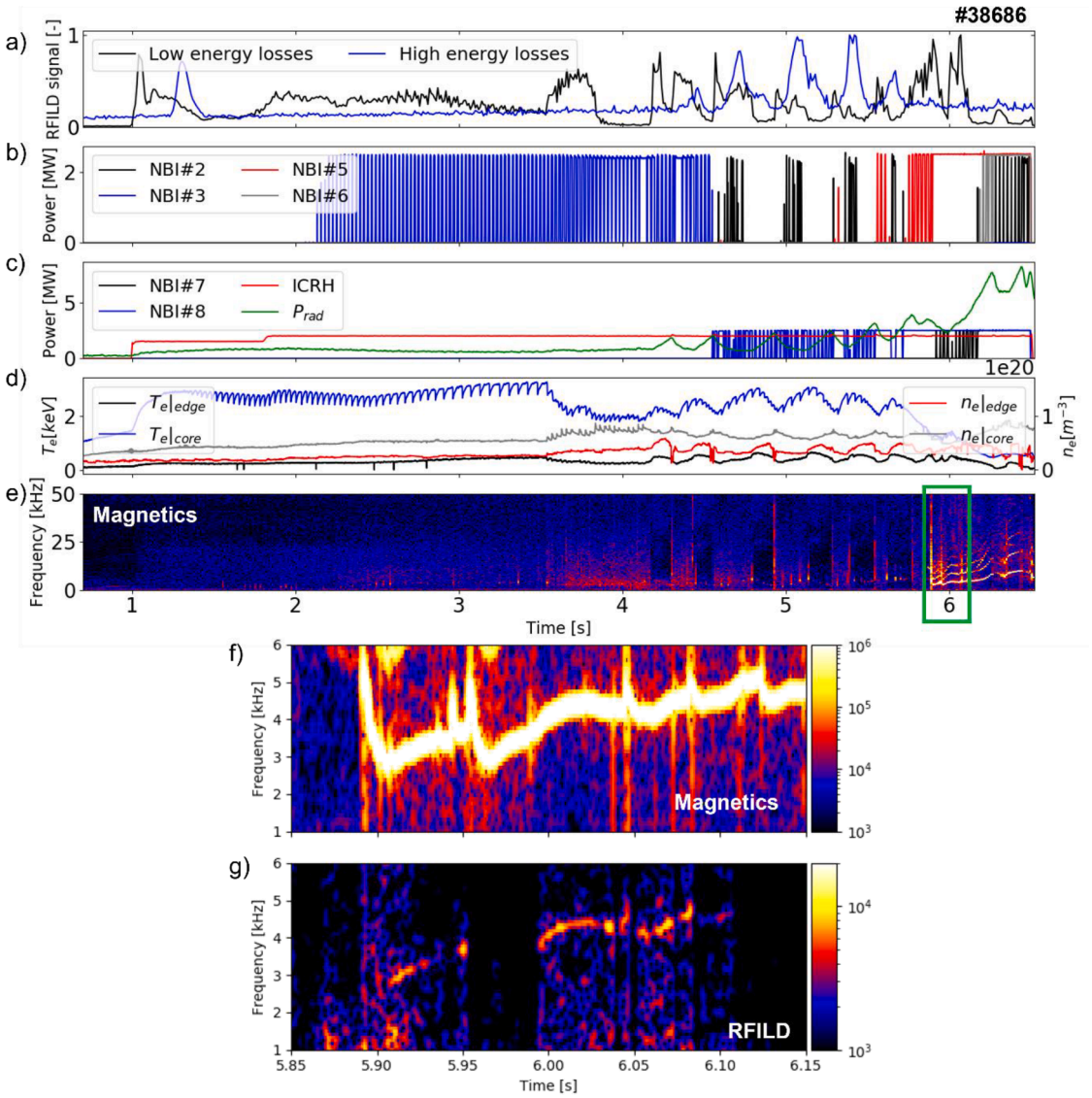

Fig. 7. Time traces corresponding to #38686: (a) RFILD signal. (b) NBIs #2, #3, #5 and #6. (c) NBIs #7 and #8, ICRH heating and radiated power. (d) Electron temperature and density evolution. (e) Magnetics spectrogram. (f) RFILD spectrogram.

in Fig. 3.

The double collimator probe head can be easily rotated to measure in forward I_p/B_t configuration. This opens the possibility of measuring the inner leg of banana particles in the extra collimator in comparison with the single collimator design. Fewer losses are expected due to the orbit topology, so the impact of adding an extra collimator in forward I_p/B_t is less significant than in its reversed counterpart.

The addition of a second collimator requires the manufacturing of a new graphite probe head (shown in Fig. 9(a)). Normally, in a single collimator probe head, a D-shaped slot is performed on the probe head side to reduce the self-shadowing, while the other side is left circular. In this double collimator configuration, a symmetric D-shape design is followed as self-shadowing must be avoided in both cases. The scintillator size is constrained by the port diameter. The double D-shape and the scintillator maximum size provoke an overlap of the strikemaps corresponding to each collimator (Fig. 9(b)). The origin of the signal in the scintillator can still be elucidated as:

- The NBI signal is expected to have a ρ_L of ~3 cm (in a standard $|B_t| =$ 2.5 T shot). There is almost no overlapping at this ρ_L.
- The ICRH signal features a spot with a long spread in ρ_L but narrow in pitch. Therefore, the spot "points" towards their origin collimator. This effect is also observed to a lesser extent in NBI spots as the ρ_L resolution is better at small gyroradii as shown in Fig. 3(a).

5. Conclusions

A FILD detector for operation in reversed I_p/B_t in AUG (RFILD) has been designed and commissioned, thus, expanding the operational space of the FILD suite. The collimator geometry was optimised for the NBI injection energy (93 keV) and for trapped particles using the FILDSIM code. The usage of IR cameras during the detector commissioning ensured that the detector probe head is safe under normal operational conditions.

First NBI measurements during an NBI scan (sources 2 to 7 in #38673) show NBI losses in RFILD in all the scanned sources. NBI#8 produces the most losses and NBI#6, the least. All sources produce a high pitch (~80°) spot, and sources #2, #3, #4, #5 and #8 also produce a 60° spot. The latter has been identified as prompt-losses.

The first ICRH measurements were obtained in a series of 2.5 T and −0.8 MA shots. Shot #38686 features two phases, a pure ICRH phase

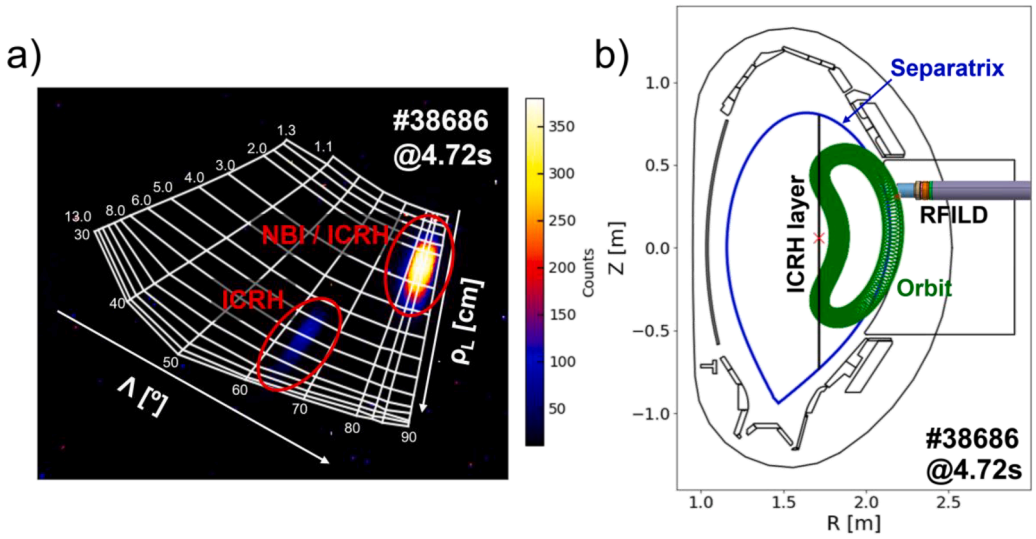

Fig. 8. (a) RFILD frame with a low and a high ρ_L spot. (b) Poloidal cross-section with a high-ρ_L orbit (in green) passing by the ICRH layer (in black). Orbit has been traced back from the RFILD pinhole. Both figures belong to #38686 at $t = 4.72$ s.

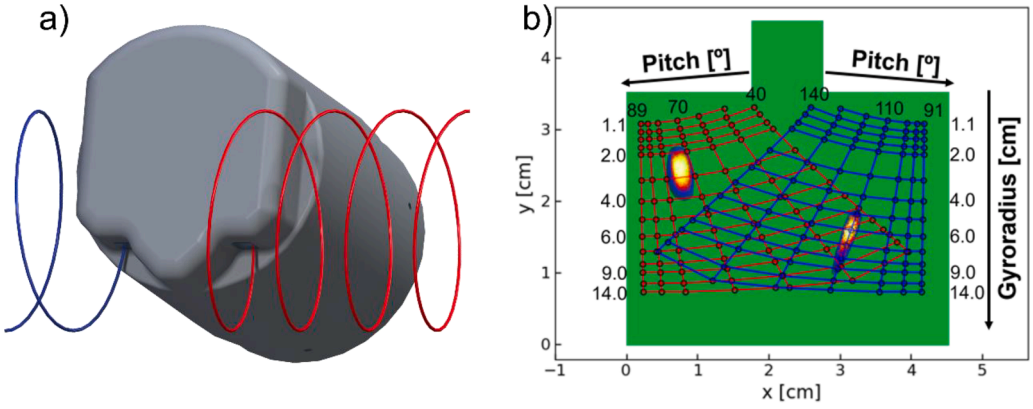

Fig. 9. (a) CAD design of the double collimator probe head. (b) Double collimator RFILD strikemap.

and a second phase with ICRH and NBI. In the first phase, high- (~1200 keV) and low-energy (~100 keV) ICRH, likely, protons are measured. The second phase features again a low- and a high-ρ_L spot, but this time the temporal coexistence of NBI and ICRH ions does not allow discerning if the low-ρ_L spot comes from NBI deuterons, from ICRH-accelerated hydrogen or from ICRH further acceleration of NBI deuterons. Due to its large ρ_L, the second spot is an ICRH spot, but the species that originates it cannot be determined. During this shot, a ($m = 2$, $n = 1$) NTM was observed in the RFILD fast-channel spectrogram.

A double collimator has been designed for a future reversed I_p/B_t campaign. This will allow the simultaneous measurement of co- and counter-current losses and expand the measurable Λ range. This configuration will be of significant importance for ITER, where the generated α particles are expected to arrive from both directions due to the isotropic nature of the fusion-born alphas.

Declaration of Competing Interest

The authors declare that they have no known competing financial interests or personal relationships that could have appeared to influence the work reported in this paper.

The authors declare the following financial interests/personal relationships which may be considered as potential competing interests:

Data availability

Data will be made available on request.

Acknowledgments

The authors gratefully acknowledge the financial support of the European Research Council (ERC) under the European Union's Horizon 2020 research and innovation programme (Grant Agreement No. 805162). This project has been developed in the framework of the 2020 Leonardo Grants for Researchers and Cultural Creators of the BBVA Foundation (Grant Agreement No 2020/00001464). This work has been carried out within the framework of the EURO fusion Consortium, funded by the European Union via the Euratom Research and Training Programme (Grant Agreement No 101052200 – EUROfusion). Views and opinions expressed are however those of the author(s) only a do not necessarily reflect those of the European Union or the European Commission. Neither the European Union nor the European Commission can be held responsible for them.

References

[1] M. García-Muoz, H.U. Fahrbach, H. Zohm, Scintillator based detector for fast-ion losses induced by magnetohydrodynamic instabilities in the ASDEX upgrade tokamak, Rev. Sci. Instrum. 80 (2009), https://doi.org/10.1063/1.3121543.

[2] R.K. Fisher, D.C. Pace, M. García-Muoz, W.W. Heidbrink, C.M. Muscatello, M. A. van Zeeland, Y.B. Zhu, Scintillator-based diagnostic for fast ion loss measurements on DIII-D, Rev. Sci. Instrum. (2010), https://doi.org/10.1063/1.3490020.

[3] J.F. Rivero-Rodriguez, M. Garcia-Munoz, R. Martin, J. Galdon-Quiroga, J. Ayllon-Guerola, R.J. Akers, J. Buchanan, D. Croft, D. Garcia-Vallejo, J. Gonzalez-Martin, D. Harvey, K.G. McClements, M. Rodriguez-Ramos, L. Sanchis, A rotary and reciprocating scintillator based fast-ion loss detector for the MAST-U tokamak, Rev. Sci. Instrum. 89 (2018), https://doi.org/10.1063/1.5039311.

[4] J. Gonzalez-Martin, M. Garcia-Munoz, A. Herrmann, J. Ayllon-Guerola, J. Galdon-Quiroga, A. Kovacsik, P. Leitenstern, T. Lunt, J.F. Rivero-Rodriguez, B. Sieglin, S. Zoletnik, J. Dominguez, First measurements of a magnetically driven fast-ion loss detector on ASDEX Upgrade, J. Instrum. (2019), https://doi.org/10.1088/1748-0221/14/11/C11005. Institute of Physics Publishing.

[5] J. Gonzalez-Martin, J. Ayllon-Guerola, M. Garcia-Munoz, A. Herrmann, P. Leitenstern, P. de Marne, S. Zoletnik, A. Kovacsik, J. Galdon-Quiroga, J. Rivero-Rodriguez, M. Rodriguez-Ramos, L. Sanchis-Sanchez, J. Dominguez, First measurements of a scintillator based fast-ion loss detector near the ASDEX Upgrade divertor, Rev. Sci. Instrum. 89 (2018), https://doi.org/10.1063/1.5038968.

[6] D.G. Whytea, A.E. Hubbard, J.W. Hughes, B. Lipschultz, J.E. Rice, E.S. Marmar, M. Greenwald, I. Cziegler, A. Dominguez, T. Golfinopoulos, N. Howard, L. Lin, R. M. McDermottb, M. Porkolab, M.L. Reinke, J. Terry, N. Tsujii, S. Wolfe, S. Wukitch, Y. Lin, I-mode: an H-mode energy confinement regime with L-mode particle transport in Alcator C-Mod, Nucl. Fusion. 50 (2010), https://doi.org/10.1088/0029-5515/50/10/105005.

[7] E. Viezzer, Access and sustainment of naturally ELM-free and small-ELM regimes, Nucl. Fusion 58 (2018), https://doi.org/10.1088/1741-4326/aac222.

[8] K.H. Burrell, M.E. Austin, D.P. Brennan, J.C. DeBoo, E.J. Doyle, C. Fenzi, C. Fuchs, P. Gohil, C.M. Greenfield, R.J. Groebner, L.L. Lao, T.C. Luce, M.A. Makowski, G. R. McKee, R.A. Moyer, C.C. Petty, M. Porkolab, C.L. Rettig, T.L. Rhodes, J.G. Rost, B.W. Stallard, E.J. Strait, E.J. Synakowski, M.R. Wade, J.G. Watkins, W.P. West, Quiescent double barrier high-confinement mode plasmas in the DIII-D tokamak, Phys. Plasmas 8 (2001) 2153–2162, https://doi.org/10.1063/1.1355981.

[9] E. Hirvijoki, O. Asunta, T. Koskela, T. Kurki-Suonio, J. Miettunen, S. Sipilä, A. Snicker, S. Äkäslompolo, ASCOT: solving the kinetic equation of minority particle species in tokamak plasmas, Comput. Phys. Commun. 185 (2014) 1310–1321, https://doi.org/10.1016/j.cpc.2014.01.014.

[10] J. Galdon-Quiroga, M. Garcia-Munoz, M. Salewski, A.S. Jacobsen, L. Sanchis-Sanchez, M. Rodriguez-Ramos, J. Ayllon-Guerola, J. Garcia-Lopez, J. Gonzalez-Martin, M.C. Jimenez-Ramos, J.F. Rivero-Rodriguez, E. Viezzer, Velocity-space sensitivity and tomography of scintillator-based fast-ion loss detectors, Plasma Phys. Control. Fusion 60 (2018), https://doi.org/10.1088/1361-6587/aad76e.

[11] J.F. Rivero-Rodriguez, M. Garcia-Munoz, J. Galdon-Quiroga, J. Gonzalez-Martin, J. Ayllon-Guerola, D. Garcia-Vallejo, R. Martin, K.G. McClements, L. Sanchis, S. Zoletnik, A fast model to resolve the velocity-space of fast-ion losses detected in ASDEX Upgrade and MAST Upgrade, J. Instrum. (2019), https://doi.org/10.1088/1748-0221/14/09/C09015. Institute of Physics Publishing.

[12] M. Rodríguez-Ramos, M.C. Jiménez-Ramos, M. García-Muñoz, J. García López, Temperature response of several scintillator materials to light ions, Nucl. Instrum. Methods Phys. Res. B 403 (2017) 7–12, https://doi.org/10.1016/j.nimb.2017.04.084.

[13] J. Galdon-Quiroga, M. Garcia-Munoz, L. Sanchis-Sanchez, M. Mantsinen, S. Fietz, V. Igochine, M. Maraschek, M. Rodriguez-Ramos, B. Sieglin, A. Snicker, G. Tardini, D. Vezinet, M. Weiland, L.G. Eriksson, Velocity space resolved absolute measurement of fast ion losses induced by a tearing mode in the ASDEX Upgrade tokamak, Nucl. Fusion. 58 (2018), https://doi.org/10.1088/1741-4326/aaa33b.

[14] B. Sieglin, M. Faitsch, A. Herrmann, B. Brucker, T. Eich, L. Kammerloher, S. Martinov, Real time capable infrared thermography for ASDEX Upgrade, Rev. Sci. Instrum. 86 (2015), https://doi.org/10.1063/1.4935580.

[15] J. Hidalgo-Salaverri, J. Gonzalez-Martin, J. Ayllon-Guerola, M. Garcia-Munoz, B. Sieglin, J. Galdon-Quiroga, D. Silvagni, E. Viezzer, J. Rueda-Rueda, T. Lunt, A. Herrmann, Thermo-mechanical limits of a magnetically driven fast-ion loss detector in the ASDEX Upgrade tokamak, J. Instrum. 17 (2022) C02020, https://doi.org/10.1088/1748-0221/17/02/c02020.

[16] G. Glockler, The heat of sublimation of graphite and the composition of carbon vapor, J. Chem. Phys. 22 (1954) 159–161, https://doi.org/10.1063/1.1740023.

[17] M. Weiland, R. Bilato, B. Geiger, P.A. Schneider, G. Tardini, M. Garcia-Munoz, F. Ryter, M. Salewski, H. Zohm, Phase-space resolved measurement of 2nd harmonic ion cyclotron heating using FIDA tomography at the ASDEX Upgrade tokamak, Nucl. Fusion. 57 (2017), https://doi.org/10.1088/1741-4326/aa7e0a.

[18] L. Stipani, A fast ion loss detector for the TCV tokamak, 2021. 10.5075/epfl-thesis-8327.